

Towards the hydrothermal growth of hierarchical cauliflower-like TiO₂ anatase structures

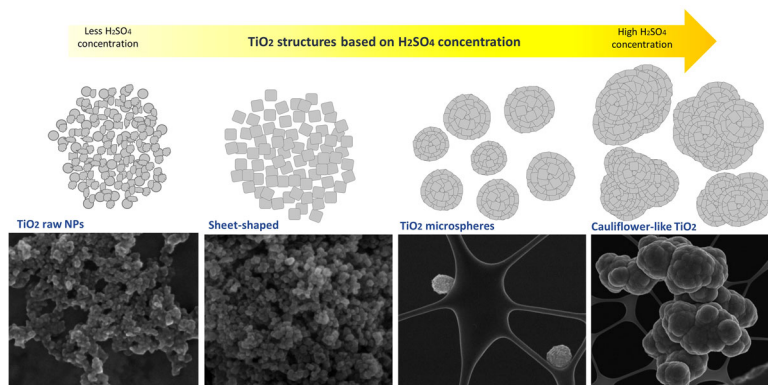
Imperio Anel Perales-Martínez¹ · Vicente Rodríguez-González²

Received: 14 July 2016 / Accepted: 13 October 2016 / Published online: 28 October 2016
© Springer Science+Business Media New York 2016

Abstract TiO₂ anatase nanostructure-based hierarchical spheres were synthesized by using a facile microwave-assisted hydrothermal method. H₂SO₄ was used as both phase inducer for the formation of anatase and capping agent to promote the self-assembly of cauliflower-like spheres. The hydrothermal synthesis was carried out at 180 °C for 2 h from an acid colloidal solution of titanium tetraisopropoxide, at pH < 2. The relationship between morphology and structure was studied by the means of X-ray diffraction, high-resolution transmission electron microscopy, scanning electron microscopy, Fourier transform infrared spectroscopy, X-ray photoelectron spectroscopy, nitrogen adsorption and

ultraviolet-visible spectroscopy analyses. The results revealed that the acid concentration is a key factor to the controlled hydrothermal aggregation of TiO₂ anatase faceted-like nanoparticles, leading to hierarchical cauliflower-like structures. The microspheres consist of hierarchical structures of sheet-shaped TiO₂ anatase particles with exposed {001} and {101} facets. The nanostructures grow in preferential directions to become in sheet-shaped, by an oriented attachment mechanism. The sulphate groups anchored on the surface and detected by X-ray photoelectron spectroscopy, help the hydrothermal formation of hierarchical spheres and then the cauliflower-like morphology.

Graphical Abstract



Keywords Hierarchical cauliflower-like structures · H₂SO₄ as capping agent · Exposed facets · Microwave-assisted hydrothermal method · Acid colloidal solution

✉ Imperio Anel Perales-Martínez
imperio.anel@gmail.com
anel.perales@itesm.mx

¹ Instituto Tecnológico y de Estudios Superiores de Monterrey, Campus Monterrey, Av. Garza Sada 2501 Sur, Tecnológico, C.P. 64849 Monterrey, Nuevo León, Mexico

² División de Materiales Avanzados, IPICYT (Instituto Potosino de Investigación Científica y Tecnológica), Camino a la Presa San José 2055 Col. Lomas 4a. sección C.P., San Luis Potosí 78216, Mexico

1 Introduction

Shape-controlled synthesis of nanocrystals with exposed reactive facets is of great importance for both fundamental studies and technological applications such as photocatalysis, smart surface coatings, dye-sensitive solar cells, photochromic devices, gas sensing, energy storage in electrochemical capacitors and hydrogen production [1–3]. Anatase titanium dioxide (TiO_2) is the most studied metal oxide due to its physicochemical properties, which are directly dependent on its size and shape [4, 5]. The high surface area facilitates the reaction/interaction between TiO_2 and the interacting medium, which mainly occurs on the surface or at the interface and strongly depends on the material surface area [5]. For anatase, theoretical studies indicate that the order of the average surface energies is $\gamma\{001\}$ ($0.90 \text{ J}\cdot\text{m}^{-2}$) $>$ $\gamma\{100\}$ ($0.53 \text{ J}\cdot\text{m}^{-2}$) $>$ $\gamma\{101\}$ ($0.44 \text{ J}\cdot\text{m}^{-2}$) [6, 7]. The most stable and frequently observed surface on anatase micro and nanostructures has (101) orientation because of the minimization of the surface energy of the crystals [8–10]. On the contrary, the growth of {001} facets anatase crystals diminish rapidly due to high surface energy. Through conventional synthesis methods of anatase TiO_2 , several researches have obtained anatase crystals without a controlled growth of anatase crystals [11–13]. Lately, in order to obtain nanocrystalline TiO_2 with the specific morphology of exposed facets, several investigations have been carried out [9, 10, 14–17]. Capping agents are used to synthesize nanoparticles in desired configuration as size, shape, distribution/dispersion, etc. Many reagents, both acid and alkaline media (HF , NH_4F , EDTA , NaOH , HCl , PVP , H_2SO_4 , etc.), have been used as capping agents during the growth process to obtain anatase crystals with the specific morphology of exposed facets [18–24]. However, many of the fluorine-containing compounds are highly toxic and corrosive and the removal of F^- from surface exposed facets is difficult due to strong interactions between F^- and TiO_2 facets [24–28]. In order to avoid the use of fluorinated compounds, the development of a new synthesis route to achieve anatase TiO_2 crystals with exposed high energy facets is highly desirable. In this regard, H_2SO_4 has been used as capping agent to obtain TiO_2 with the specific morphology of exposed facets avoiding the use of fluorinated compounds [24]. On the other hand, the shape of the obtained particles not only depends on the capping agent, but also on the colloidal solution conditions of the synthesis method. Hydrothermal synthesis is a heterogeneous reaction in presence of aqueous solvents under high pressure and temperature, through conventional distribution of energy, to dissolve and recrystallize materials that are insoluble under normal conditions. Microwave-assisted hydrothermal method (MWA-H) offers the same characteristics than conventional

hydrothermal method, the advantage is that it employs shorter reaction times due to the electromagnetic waves of high frequency which have the capacity to focus their energy causing that dipolar molecules try to be in phase with the field. However, its movement is restricted by resistance forces generating heat. For this reason, MWA-H yields a fast velocity of response and short reaction times being reflected in low energy consumption [29, 30].

In the present work, a practical MWA-H for the synthesis of hierarchical cauliflower-like TiO_2 anatase structures from the aggregation of spheres formed of exposed facets sheet-shaped particles, using titanium tetraisopropoxide (IV) as titanium precursor and H_2SO_4 as capping agent, is reported. Our work provides new insights on the control of the morphology of anatase particles from sol acid solution in a short reaction time.

2 Materials and methods

2.1 Materials

Titanium (IV) tetraisopropoxide (TTIP, $>97\%$, Sigma Aldrich), sulfuric acid ($>96\%$, Fermont) and deionized water ($>17 \text{ M}\Omega \text{ cm}$) from a Millipore Milli-Q system were used throughout the experiments.

2.2 Synthesis of TiO_2 anatase hierarchical spheres

The products were prepared by a MWA-H involving an aqueous colloidal solution of Titanium tetraisopropoxide and sulfuric acid. The schematic layout of the synthesis process is illustrated in Fig. 1. As part of a typical experiment, 3 mL of titanium tetraisopropoxide were suspended in 50 mL of sulfuric acid solution ($\text{pH} < 2$) for 1 h. The mixture was placed in a 150-mL Teflon vessel and heated under microwave irradiation by using a microwave reactor (model MWO-1000S, EYELA Japan). The temperature was fixed at 180°C for 2 h, 400 rpm and a maximum variable microwave irradiation power of 150 W. Following that, the hydrothermal aging gel was naturally cooled down to room temperature. The white precipitate obtained, was centrifuged at 4000 rpm for 5 min, filtered and washed with deionized water. Finally, it was dried at 80°C for 12 h. Sulfuric acid concentrations were varied from 0.0 to 3.5 mol/L. The name of the synthesized samples are X- TiO_2 , where X means the sulfuric acid concentration.

2.3 Characterization

The structural characterization of the obtained oxides was carried out by X-ray powder diffraction using a Bruker D8 Advance diffractometer with $\text{CuK}\alpha$ radiation ($\lambda = 1.54 \text{ \AA}$).

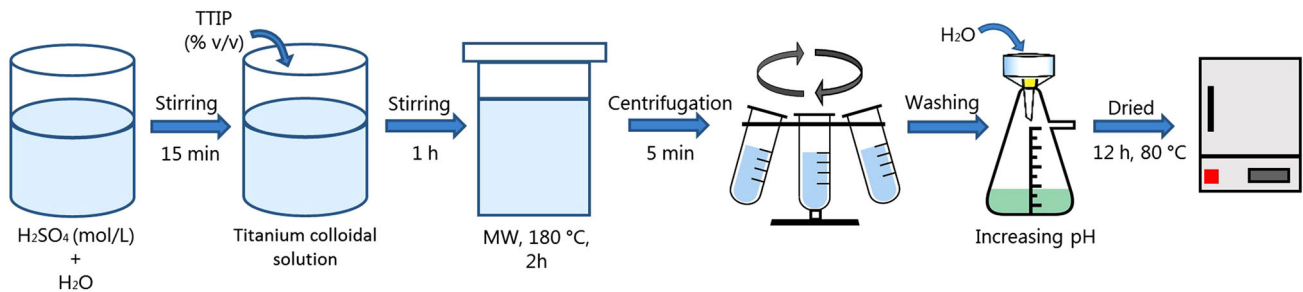


Fig. 1 Schematic presentation of synthesis procedure of hierarchical cauliflower-like TiO₂ anatase structures

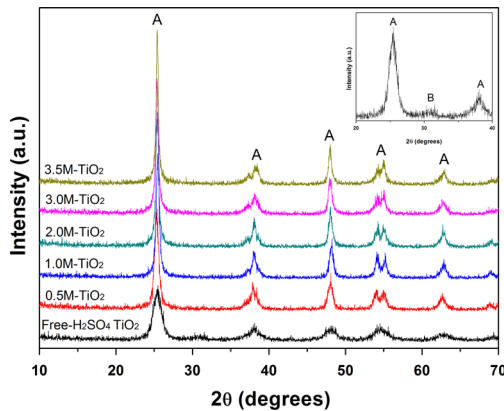


Fig. 2 XRD patterns of samples synthesized with different of H₂SO₄ concentrations

The morphology and elemental composition analyses were performed by energy dispersive X-ray spectroscopy (EDS) in a FE-SEM (FE-SEM, Helios Double Beam 600 high resolution, operated at 5 kV with an opening of 86 pA). Crystallographic morphology and lattice structures were observed using a high resolution transmission electron microscopy (HR-TEM, FEI Tecnai F30, equipped with a tungsten field emission gun operated at 300 keV). Energy gap values were estimated by means of a UV–vis spectrophotometer Cary-5000 equipped with a diffuse reflectance system. The energy band gap (E_g) was calculated using the equation $\alpha(h\nu) = A(h\nu - E_g)^{n/2}$, where α is the absorption coefficient, $h\nu$ is the photon energy, A is a constant and $n = 2$ when represents a direct transition between valence band and conduction band. For the estimation of E_g from the UV–vis spectra, a straight line was extrapolated from the $F(R)$ curve to the abscissa axis. When α has a value of zero, then $E_g = h\nu$ [31]. The surface composition was investigated by X-ray photoelectron spectroscopy (XPS, K-Alpha Thermo Scientific with an X-ray MgK α source operated at 12 kV and 6 mA). IR spectra, in the range between 4000– 525 cm^{-1} , were recorded on a Thermo Nicolet 6700 spectrophotometer using the KBr pellet technique. On the other hand, N₂ adsorption–desorption measurements were carried out using a Nova 3000 gas-sorption

Table 1 Physical properties of the different synthesized samples

Sample	Crystal size (nm)	Surface area (m ² /g)	Energy (eV)	λ (nm)
Free-H ₂ SO ₄ -TiO ₂	13.5	177	3.26	380
0.5M-TiO ₂	24.4	100	3.28	378
1.0M-TiO ₂	33.0	113	3.26	380
2.0M-TiO ₂	34.7	65	3.26	380
3.0M-TiO ₂	36.4	86	3.23	383
3.5M-TiO ₂	56.0	73	3.22	385

system, which has the flexibility to implement multiple methods of analysis at the same time as multipoint BET and pore size distribution by the BJH (Barrett-Joyner-Halenda) method of desorption isotherms.

3 Results and discussion

3.1 Effect of H₂SO₄ concentration of colloidal solution

XRD patterns of the samples synthesized varying the H₂SO₄ concentrations are shown in Fig. 2. Reflections marked as A and B correspond to the anatase (JCPDS 78-2486) and brookite TiO₂ crystalline phases (JCPDS 16-0617), respectively, where anatase is the main crystalline phase. For Free-H₂SO₄ TiO₂ sample additionally to anatase phase, reflections corresponding to the brookite orthorhombic structure show two small peaks at around 30.2° and 32° in 2 θ (Fig. 2, inset). It is noteworthy that the most intense peak of the brookite phase (120) is located at 25.3°, which is the same position that the most intense anatase phase (101) peak. Due to the overlapping of the two main peaks of these two phases, it is not possible to observe the main peak of the brookite crystalline phase. However, the peaks observed at 30.2° and 32° in 2 θ give evidence of the coexisting phases in the synthesis performed in absence of sulfuric acid. It is observed that all synthesized samples with H₂SO₄ exhibit only the TiO₂ anatase phase. Moreover,

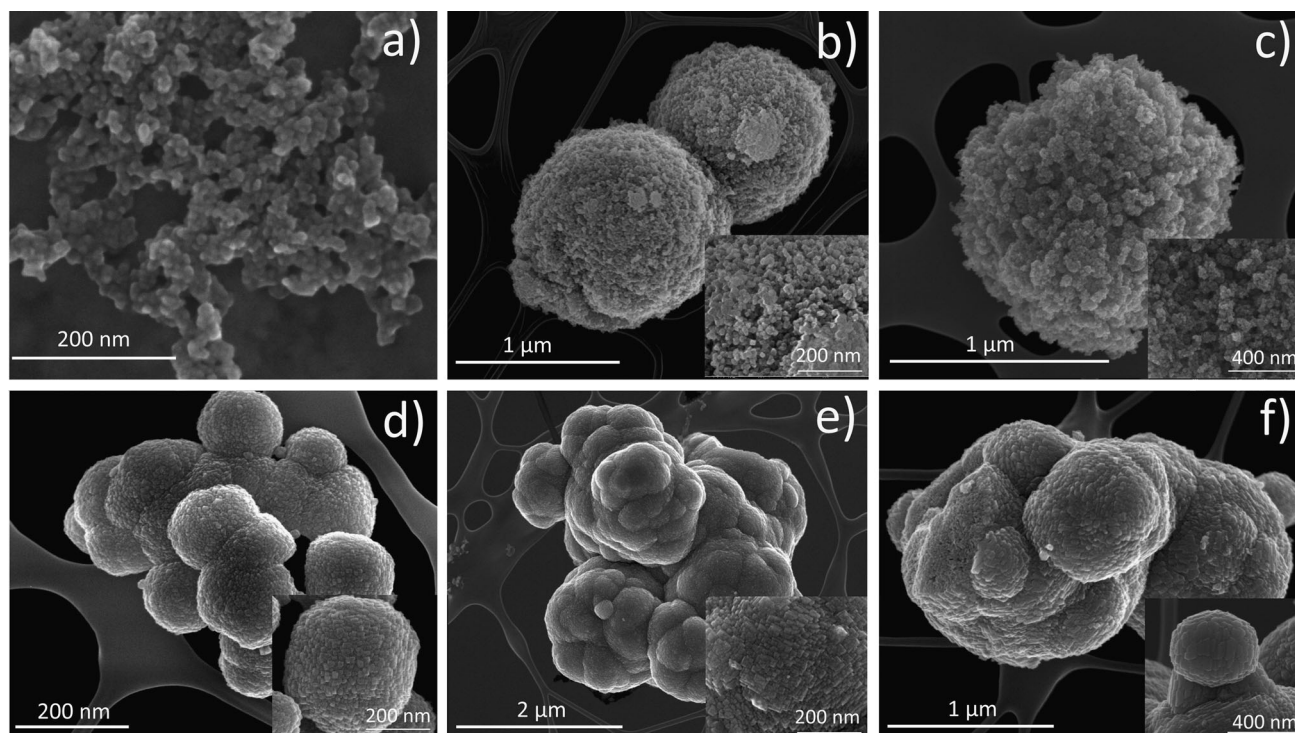


Fig. 3 FE-SEM images of **a** Free- H_2SO_4 TiO_2 , **b** 0.5M- TiO_2 , **c** 1.0M- TiO_2 , **d** 2.0M- TiO_2 , **e** 3.0M- TiO_2 , **f** 3.5M- TiO_2 synthesized samples by MWA-H for 2 h

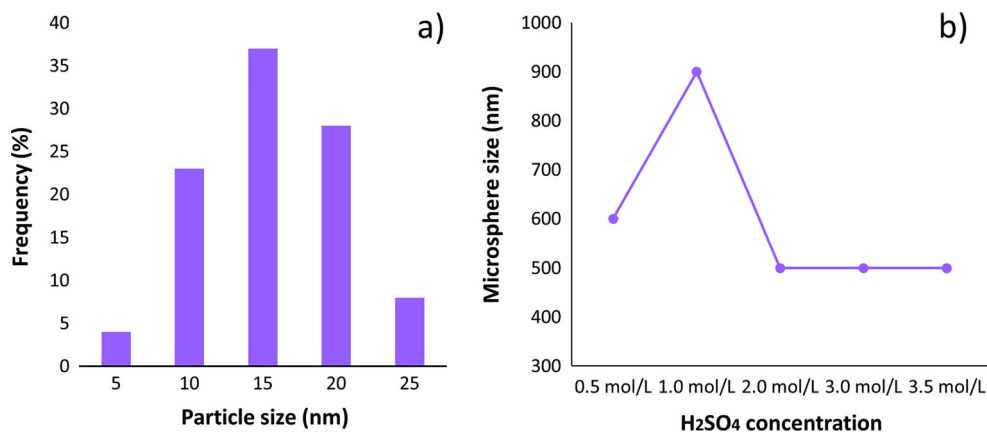


Fig. 4 **a** Distribution of anatase particle size of Free- H_2SO_4 TiO_2 and **b** microspheres sizes of 0.5 to 3.5 mol/L sulfuric acid samples

the relative intensity of the anatase peak does not increase with the increasing acid concentration in the reaction colloidal solutions. These results suggest that the addition of H_2SO_4 during the synthesis exerts an effect as inducer-agent to the formation of the anatase phase, constraining the formation of any other titanium dioxide phase. Scherrer's equation was used to calculate the crystal size of anatase phase: $D = k\lambda/\beta\cos\theta$, where D is the crystallite particle size, k is a constant of 0.9, λ is the X-ray wavelength (1.54 Å), β is the full width at half maximum, and θ is the Bragg angle using the {101} reflection peak [32]. Results of

average crystal size showed an increase in crystal size as the acid concentration increases (Table 1).

The FE-SEM images of TiO_2 synthesized at different H_2SO_4 concentrations and free of H_2SO_4 are shown in Fig. 2. It can be noted that the Free- H_2SO_4 TiO_2 sample consists of irregular particles and does not have a well-defined morphology (Fig. 3a). The size of these particles was found in the range from 10 to 20 nm as shown in Fig. 4a. Nevertheless, a difference is observed for samples with different H_2SO_4 concentrations. The lowest concentration (0.5 mol/L H_2SO_4) particles tend to aggregate

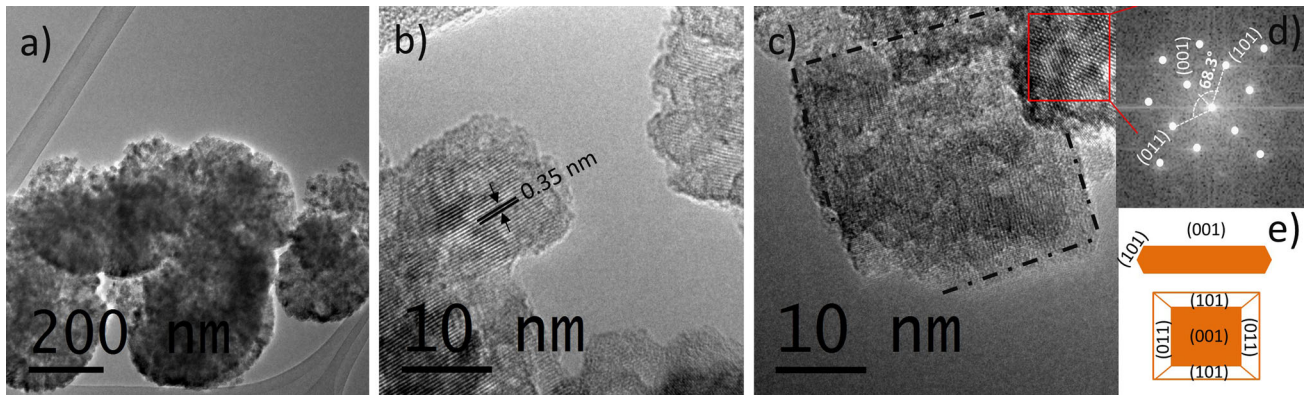


Fig. 5 **a** TEM image of anatase TiO_2 hierarchical spheres, **b, c** HRTEM images of single crystal of anatase, **d** FFT pattern recorded from the dotted box area in **c**, **e** Representative schema of single crystal of anatase with exposed facets $\{001\}$ and $\{101\}$

and ultimately form microspheres which are composed of agglomerates of pseudo-spherical particles. These microspheres consist of integrated particles with sizes in the order of nanometers (Fig. 3b). The size of the microspheres was ~ 600 nm (Fig. 3b inset, Fig. 4b). For a concentration of 1 mol/L H_2SO_4 , it was observed that the particles aggregation increased and therefore, the average size of the microspheres increased to ~ 900 nm (Fig. 3c inset, Fig. 4b). From a concentration of 2 mol/L H_2SO_4 , agglomerates of self-assembled particles were observed (Fig. 3d). The size of the microspheres ranges from 500 nm. This slight decrease in the microsphere size is due to the nanosized particles that set up the microspheres, which have a sheet-shaped morphology (see Fig. 3d inset), and this contributes to the assembling the particles more orderly until forming a well-shaped microsphere. With increasing concentrations (3.0 and 3.5 mol/L) it is shown that there is a aggregation of microspheres on the surface of other microspheres, resulting in a cauliflower-like morphology ($\sim 1 \mu\text{m}$) (Figs. 3e and f), however the microsphere sizes is maintained in ~ 500 nm as shown in Fig. 4b. This fact reveals that the TiO_2 anatase assumes the hierarchical cauliflower-like structure composed of numerous microspheres which further are composed of anatase nanoparticles. According to what was observed by scanning microscopy, the acid concentration exerts a compacting effect, determining the overall morphology of the TiO_2 anatase structures. As noted in the FE-SEM images, an increase in the H_2SO_4 concentration promoted the self-assembly from particles to finally form microspheres. At the same time, the sulfuric acid acts as a capping agent for the formation of sheet-shaped particles during hydrothermal aging. Similar results were found by Zhao et al. [24], who reported that H_2SO_4 serves as both an inducer agent in the synthesis of titanium dioxide to form the anatase phase and capping agent to promote the formation of self-assembled microspheres which are formed by sheet-shaped particles with exposed $\{001\}$ faces.

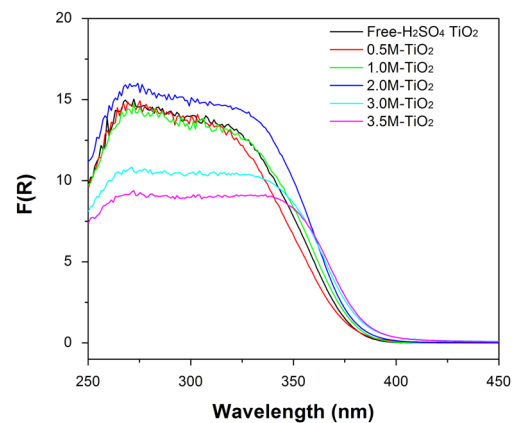


Fig. 6 Bandgap energy of the synthesized samples at different concentrations of acid

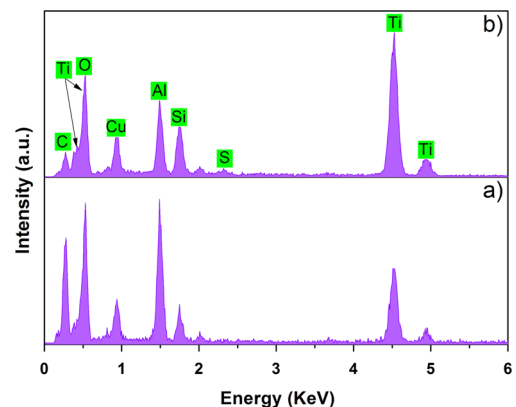


Fig. 7 Spectrum of EDS analyses of **a** Free- H_2SO_4 TiO_2 and **b** 2.0M- TiO_2 samples

TEM images of 2.0M- TiO_2 sample confirm that microspheres are composed of nanoparticles which have a sheet-shaped morphology (Fig. 5a). The HRTEM image displays a single d-spacing of 0.35 nm that agrees well with the standard spacing of 0.35 nm between the (101) lattice

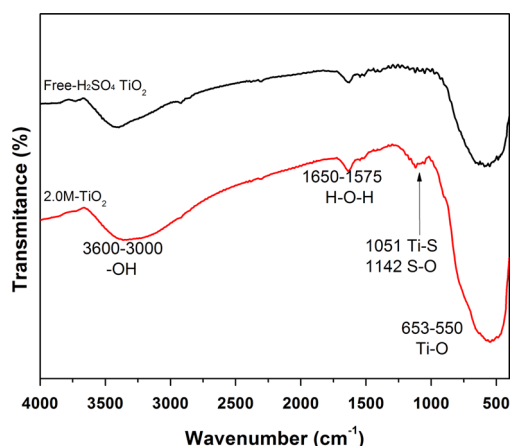


Fig. 8 FT-IR spectra for powders of Free-H₂SO₄-TiO₂ and 2.0M-TiO₂

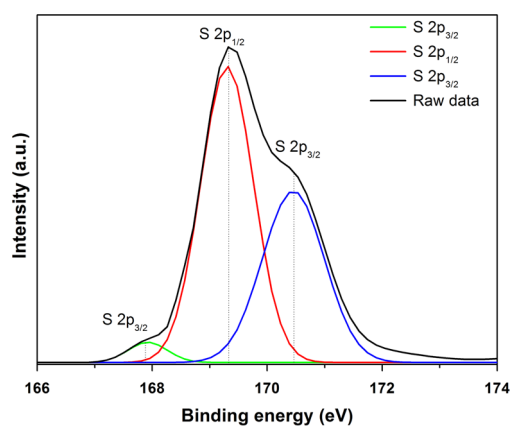


Fig. 9 Representative XPS spectra of anatase TiO₂ microspheres self-assembled

planes of the TiO₂ anatase crystal as is shown in Fig. 3b. The equal-thickness fringes observed at the edge of the square-shaped particle indicate the presence of slopes due to {101} facets. The particles that make up the microspheres are single crystals with well-defined borders and edges as shown in Fig. 5c. The corresponding FFT (Fast-Fourier transform) pattern (Fig. 5d) obtained from a selected area in Fig. 5c reveals an angle of 68.3°, which is consistent with the interfacial angle between (001) and (101), suggesting that the particle exhibits flat surfaces of {001} and {101}. Fig. 5e shows a schematic representation of a single crystal of TiO₂ anatase with flat {001} and {101} surfaces.

On the basis of HRTEM images as well as of the crystallographic symmetries of anatase, it can be easily confirm that the sheet-shaped particles of the TiO₂ crystals have eight {101} and two {001} facets at top/bottom surfaces. These particles are self-assembled to form the microspheres. Similar results of exposed TiO₂ facets have been found by other authors [3, 7, 33, 34].

The band gap energy values were calculated from UV–Vis diffuse reflectance spectroscopy as showed in

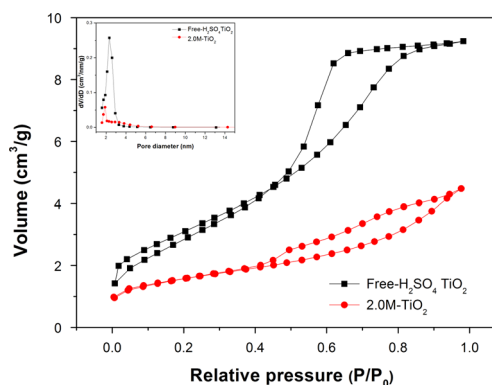


Fig. 10 N₂ adsorption/desorption isotherms of the anatase TiO₂ hierarchical spheres. The inset shows the pore size distributions calculated using the BJH method

Fig. 6 and summarized in Table 1. According to the calculated values, the TiO₂ samples with different content of acid showed analogous band gap values to n-type semiconductor TiO₂ (3.19 eV) due to its content of anatase phase. However, the slight difference between band gap values of the samples may be inferred to be a percentage of {001} facets in the surface [35], which according to SEM and TEM analysis, the morphology and exposed facets {001} are intrinsically related to the content of H₂SO₄.

On the other hand, analyses by EDS of 2.0M-TiO₂ sample gives evidence that additionally to the peaks of Ti and O, a peak corresponding to sulphur is also observed, which is due to the sulphuric acid used in the synthesis (Fig. 7). These results suggest that the method of washing with deionized water is not sufficient to remove all the acid used in the synthesis. It is noteworthy that for the other concentrations of H₂SO₄, the results were similar; remnants of sulphates were found in the samples after washing by EDS analyses. According to Ohno et al., the sulphated TiO₂ powder shows relatively high photocatalytic activity under visible and may have a wide range of applications [36].

The different concentrations of H₂SO₄ apparently influence the self-assembling of particles. These results are corroborated by FTIR analyses. Fig. 8 shows the characteristic FTIR spectra of TiO₂ synthesized in presence of H₂SO₄ and blank. For both samples, it could be observed that materials present an absorption band between 1000–1400 cm⁻¹, which is attributed to Ti–O and Ti–O–Ti bonds. However, for 2.0M-TiO₂ sample, appear bands assigned to vibrations S–O and Ti–S (1142 and 1051 cm⁻¹, respectively), which are due to sulphur-containing groups on the surface of sheet-shaped particles. As a complement of the results obtained by FTIR, XPS was performed on the 2.0M-TiO₂ sample in the region of S 2p and the corresponding spectrum is shown in Fig. 9. According to this analysis, the binding energies of sulphur were observed at

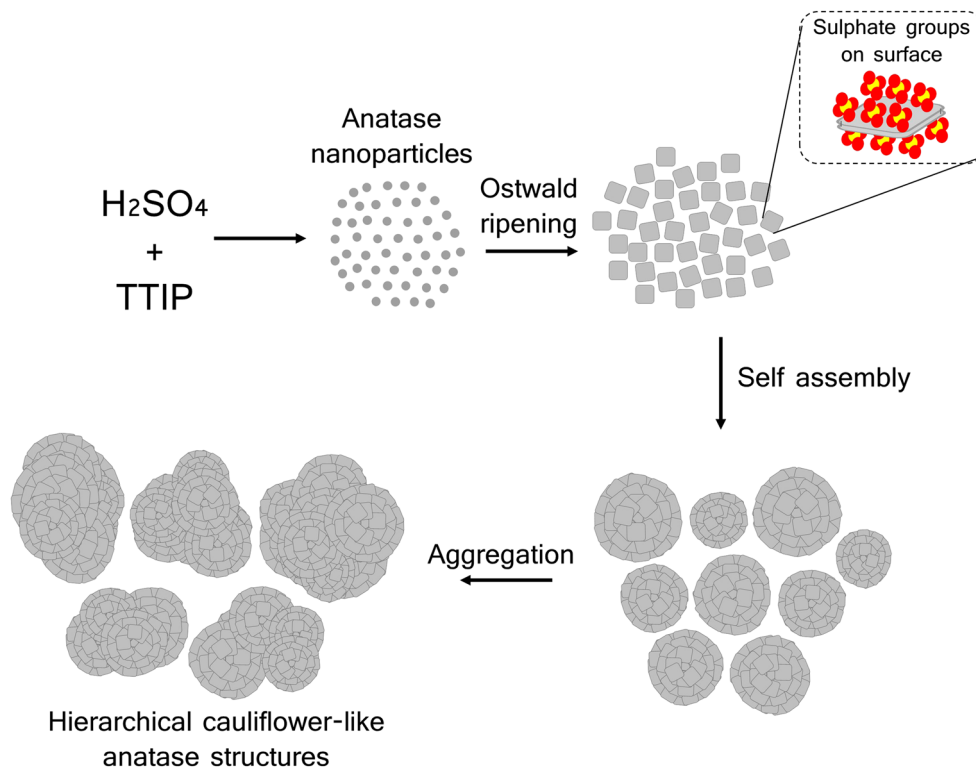
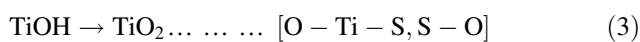
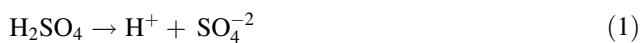


Fig. 11 Schematic illustration of the mechanism of formation of hierarchical anatase-TiO₂ structures

169.2 and 170.6 eV which are assigned to S 2p_{1/2} and S 2p_{3/2} orbitals with a separation of 1.4 eV. These energies correspond to the typical S 2p spectrum of the sulphate groups (SO₄)²⁻ [37]. Besides, Khodayari et al. reported that the peak around 169.5 eV could be attributed to the presence of surface sulphate groups [38]. Also, the small broad band located at 167.9 eV has been attributed by Khmeleva et al. to the presence of sulphate groups on the surface [39]. These groups could be responsible for the particles self-assembly to form the microspheres. No peaks for sulphur, sulphide, or sulphite groups were observed. Thus, the chemical interactions proposed between the sulfuric acid and titanium tetraisopropoxide are shown below.



On the other hand, the self-assembly of TiO₂ microspheres produces a nanoporous structure, as confirmed by the N₂ adsorption/desorption isotherm shown in Fig. 10. It gives a type-IV isotherm with a type-H2 hysteresis loop, indicating a mesoporous structure. The pore size distribution calculated from desorption isotherm by nitrogen BJH method shows a narrow range of 1.5–3.0 nm with an

average pore size of ~2.1 nm (Fig. 10 inset), which decreases due to the self-assembly of TiO₂ particles to form cauliflower-like structures (~2.4 nm for free-H₂SO₄ TiO₂ sample). The presence of sulphuric acid in the synthesis exerted a significant influence on the pore structure and surface area of the obtained products. Surface area of TiO₂ anatase synthesized in presence of H₂SO₄ is lesser than that of TiO₂ anatase free of H₂SO₄ (Table 1). These results are attributed to the formation of hierarchical structures.

As it was seen from the experiment, both the hydrothermal treatment temperature and H₂SO₄ concentration produce the synergy effect that determines the overall morphology of TiO₂ anatase nanostructures. The mechanism of formation can occur through Ostwald ripening in dissolution-recrystallization process, which the complete dissolution of smaller crystallites led to the growth of the large crystallites [40]. During the hydrothermal process, H₂SO₄ plays a key role in the formation of hierarchical structures. In the Ostwald ripening process, large crystallites grow at the expense of smaller crystallites by means of dissolution, diffusion and recrystallization. In the presence of H₂SO₄, the nanoparticles are organized as single crystals with exposed facets {001} and {101}. At higher concentrations of H₂SO₄, sulphate groups are anchored on the surface of the sheet-shaped particles, therefore the so-formed microspheres are self-assembled to hierarchical

structure through sulfite. The Fig. 11 shows the formation of hierarchical TiO₂ anatase structures. The sulphated molecules attached to sheet-shaped particles produces a negatively charged surface, hence sulphated anions must be stabilized between adjacent particles in order to maintain charge neutrality forming the hierarchical TiO₂ spheres and then its aggregation in cauliflower-like assemblies. Further, it was observed that the addition of sulfuric acid promotes the formation of anatase phase, inhibiting the formation of other titanium dioxide phases by MWA-H method in a short reaction time. The growth of hierarchical structures TiO₂-based have been reported by means of the use of capping agent in the process reaction [33, 41–44].

4 Conclusions

The synthesis of TiO₂ anatase particles with cauliflower-like morphology was achieved through the hydrothermal sol aging by microwave-assisted method without using harmful hydrofluoric acid. The use of H₂SO₄ increased the TiO₂ crystallinity degree, playing a crucial role as capping agent to promote the formation of TiO₂ anatase phase microspheres. The microspheres consist of hierarchical structures of sheet-shaped TiO₂ anatase particles with exposed {001} and {101} facets, with sizes in the order of nanometers. The concentration of sulfate ions is also a key factor to control the morphology of the cauliflower-like TiO₂ anatase structures.

Acknowledgments The authors would like to express their gratitude to CONACYT for the financial support (CB-2011/169597 and LINAN-0271911). We thank M. C. Beatriz A. Rivera Escoto, Dr. Gladis J. Labrada and Dr. Hector Silva from LINAN-IPICYT for the XRD, FE-SEM and HRTEM characterizations. I. A. Perales Martinez appreciates the CONACYT PhD scholarship.

Compliance with ethical standards

Conflict of interest The authors declare that they have no conflict of interest.

References

1. Yang HG, Liu G, Qiao SZ, Sun CH, Jin YG, Smith SC, Zou J, Cheng HM, Lu GQ (2009) Solvothermal synthesis and photo-reactivity of anatase TiO₂ nanosheets with dominant {001} facets. *J Am Chem Soc* 131:4078–4083
2. Diebold U (2003) The surface science of titanium dioxide. *Surf Sci Rep* 48:53–229
3. Liu G, Yang HG, Wang X, Cheng L, Lu H, Wang L, Lu GQ, Cheng HM (2009) Enhanced photoactivity of oxygen-deficient anatase TiO₂ sheets with dominant {001} facets. *J Phys Chem C* 113:21784–21788
4. Shengyuan Y, Peining Z, Nair AS, Ramakrishna S (2011) Rice grain-shaped TiO₂ mesostructures-synthesis, characterization and applications in dye-sensitized solar cells and photocatalysis. *J Mater Chem* 21:6541–6548
5. Chen X, Mao SS (2007) Titanium dioxide nanomaterials: synthesis, properties, modifications, and applications. *Chem Rev* 107:2891–2959
6. Liu M, Piao L, Lu W, Ju S, Zhao L, Zhou C, Li H, Wang W (2010) Flower-like TiO₂ nanostructures with exposed {001} facets: Facile synthesis and enhanced photocatalysis. *Nanoscale* 2:1115–1117
7. Yang HG, Sun CH, Qiao SZ, Zou J, Liu G, Smith SC, Cheng HM, Lu GQ (2008) Anatase TiO₂ single crystals with a large percentage of reactive facets. *Nature* 453:638–641
8. Fang WQ, Gong XQ, Yang HG (2011) On the unusual properties of anatase TiO₂ exposed by highly reactive facets. *J Phys Chem Lett* 2:725–734
9. Perales-Martínez IA, Rodríguez-González V, Lee SW (2014) Insights into nanocube-like morphological transformation of P25 by microwave-assisted hydrothermal method. *Mater Lett* 123:10–13
10. Zhang D, Li G, Wang H, Chan KM, Yu JC (2010) Biocompatible anatase single-crystal photocatalysts with tunable percentage of reactive facets. *Cryst Growth Des* 10:1130–1137
11. Montini T, Gombac V, Sordelli L, Delgado JJ, Chen X, Adami G, Fornasiero P (2011) Nanostructured Cu/TiO₂ photocatalysts for H₂ production from Ethanol and Glycerol aqueous solution. *Chem Cat Chem* 3:574–577
12. Rodríguez-González V, Obregón Alfaro S, Torres-Martínez LM, Cho SH, Lee SW (2010) Silver–TiO₂ nanocomposites: synthesis and harmful algae Bloom UV-photoelimination. *Appl Catal B: Environ* 98:229–234
13. Porkodi K, Arokiamary SD (2007) Synthesis and spectroscopic characterization of nanostructured anatase titania: a photocatalyst. *Mater Charact* 58:495–503
14. Wang W, Lu C, Ni Y, Xu Z (2013) Crystal facet growth behavior and thermal stability of {001} faceted anatase TiO₂: mechanistic role of gaseous HF and visible-light photocatalytic activity. *Cryst Eng Comm* 15:2537–2543
15. Zhang H, Wang Y, Liu P, Han Y, Yao X, Zou J, Cheng H, Zhao H (2011) Anatase TiO₂ crystal facet growth: mechanistic role of hydrofluoric acid and photoelectrocatalytic activity. *Appl Mater Interfaces* 3:2472–2478
16. Zhang H, Liu P, Li F, Liu H, Wang Y, Zhang S, Guo M, Cheng H, Zhao H (2011) Facile fabrication of anatase TiO₂ microspheres on solid substrates and surface crystal facet transformation from {001} to {101}. *Chem Eur J* 17:5949–5957
17. Liu S, Yu J, Jaroniec M (2010) Tunable photocatalytic selectivity of hollow TiO₂ microspheres composed of anatase polyhedra with exposed {001} facets. *J Am Chem Soc* 132:11914–11916
18. Ma XY, Chen ZG, Hartono SB, Jiang HB, Zou J, Qiao SZ, Yang HG (2010) Fabrication of uniform anatase TiO₂ particles exposed by {001} facets. *Chem Commun* 46:6608–6610
19. Wang D, Zhou F, Liu Y, Liu W (2008) Synthesis and characterization of anatase TiO₂ nanotubes with uniform diameter from titanium powder. *Mater Lett* 62:1819–1822
20. Wang D, Yu B, Zhou F, Wang C, Liu W (2009) Synthesis and characterization of anatase TiO₂ nanotubes and their use in dye-sensitized solar cells. *Mater Chem Phys* 113:602–606
21. Aphairaja D, Wirunmongkol T, Pavasupree S, Limsuwan P (2012) Synthesis of titanate nanotubes from thai leucosene mineral. *Procedia Eng* 32:1068–1072
22. Xia XH, Lia Y, Wang Z, Fan J, Luo YS, Jia SJ (2008) Synthesis and photocatalytic properties of TiO₂ nanostructures. *Mater Res Bull* 43:2187–2195
23. Dai Y, Cobley CM, Zeng J, Sun Y, Xia Y (2009) Synthesis of anatase TiO₂ nanocrystals with exposed {001} facets. *Nano Lett* 9:2455–2459

24. Zhao Z, Sun Z, Zhao H, Zheng M, Du P, Zhao J, Fan H (2012) Phase control of hierarchically structured mesoporous anatase TiO₂ microspheres covered with {001} facets. *J Mater Chem* 22:21965–21971
25. Wang L, Zang L, Zhao J, Wang C (2012) Green synthesis of shape-defined anatase TiO₂ nanocrystals wholly exposed with {001} and {100} facets. *Chem Commun* 48:11736–11738
26. Ong WJ, Tan LL, Chai SP, Yong ST, Mohamed AR (2014) Highly reactive {001} facets of TiO₂-based composites: synthesis, formation mechanism and characterization. *Nanoscale* 6:1946–2008
27. Lee WJ, Sung YM (2012) Synthesis of anatase nanosheets with exposed {001} facets via chemical vapor deposition. *Cryst Growth Des* 12:5792–5795
28. Li T, Tian B, Zhang J, Dong R, Wang T, Yang F (2013) Facile tailoring of anatase TiO₂ morphology by use of H₂O₂: From microflowers with dominant {101} facets to microspheres with exposed {001} facets. *Ind Eng Chem Res* 52:6704–6712
29. Yuan CAO, Hong-juan WEI, Zhi-ning XIA (2009) Advances in microwave assisted synthesis of ordered mesoporous materials. *Trans Nonferrous Met Soc China* 19:656–664
30. Shi S, Hwang JY (2003) Microwave-assisted wet chemical synthesis: Advantages, significance, and steps to industrialization. *J Miner Mater Charact Eng* 2:101–110
31. Perales-Martínez IA, Rodríguez-González V, Lee SW, Obregón S (2015) Facile synthesis of InVO₄/TiO₂ heterojunction photocatalysts with enhanced photocatalytic properties under UV–vis irradiation. *J Photochem Photobio A* 299:152–158
32. Bischoff BL, Anderson MA (1995) Peptization process in the sol-gel preparation of porous anatase (TiO₂). *Chem Mater* 7:1772–1778
33. Zheng Z, Huang B, Qin X, Zhang X, Dai Y, Jiang M, Wang P, Whangbo MH (2009) Highly efficient photocatalyst: TiO₂ microspheres produced from TiO₂ nanosheets with a high percentage of reactive {001} facets. *Chem Eur J* 15:12576–12579
34. Perales-Martínez IA, Rodríguez-González V, Obregon-Alfaro S, Lee SW (2015) Facile synthesis of decahedral particles of anatase TiO₂ with exposed {001} facets. *J Nanosci Nanotechnol* 15:7351–7356
35. Pan J, Wu X, Wang L, Liu G, Lub GQ, Cheng HM (2011) Synthesis of anatase TiO₂ rods with dominant reactive {010} facets for the photoreduction of CO₂ to CH₄ and use in dye-sensitized solar cells. *Chem Commun* 47:8361–8363
36. Ohno T, Akiyoshi M, Umebayashi T, Asai K, Mitsui T, Matsu-mura M (2004) Preparation of S-doped TiO₂ photocatalysts and their photocatalytic activities under visible light. *Appl Catal A* 265:115–121
37. Shao J, Li X, Zhang L, Qu Q, Zheng H (2013) Core-shell sulfur@polypyrrole composites as highcapacity materials for aqueous rechargeable batteries. *Nanoscale* 5:1460–1464
38. Khodayari R, Odenbrand CUI (2001) Regeneration of commercial SCR catalysts by washing and sulphation: effect of sulphate groups on the activity. *Appl Catal B Environ* 33:277–291
39. Khmeleva TN, Georgiev TV, Jasieniak M, Skinner WM, Beattie DA (2005) XPS and ToF-SIMS study of a chalcopyrite–pyrite–sphalerite mixture treated with xanthate and sodium bisulphite. *Surf Interface Anal* 37:699–709
40. Zeng HC (2007) Ostwald ripening: a synthetic approach for hollow nanomaterials. *Current Nanosci* 3:177–181
41. Yang W, Li J, Wang Y, Zhu F, Shi W, Wan F, Xu D (2011) A facile synthesis of anatase TiO₂ nanosheets-based hierarchical spheres with over 90% {001} facets for dye-sensitized solar cells. *Chem Commun* 47:1809–1811
42. Zhang H, Han Y, Liu X, Liu P, Yu H, Zhang S, Yao X, Zhao H (2010) Anatase TiO₂ microspheres with exposed mirror-like plane {001} facets for high performance dye-sensitized solar cells (DSSCs). *Chem Commun* 46:8395–8397
43. Hu X, Zhang T, Jin Z, Huang S, Fang M, Wu Y, Zhang L (2009) Single-crystalline anatase TiO₂ doped assembled micro-sphere and their photocatalytic activity. *Cryst Growth Des* 9:2324–2328
44. Luo ZH, Zhou XS, Jin B, Luo J, Xu XY, Chen LY (2015) Synthesis and characterization of novel titanium dioxide microspheres with exposed {001} facets. *Chem Lett* 44:256–258